Time-Domain Travelling-Wave Analysis of Semiconductor Optical Amplifiers based on Chirped Quantum Dot Materials

Time-Domain Travelling-Wave Analysis of Semiconductor Optical Amplifiers based on Chirped Quantum Dot Materials

Andrea Marchisio[(1)], Lorenzo Tunesi[(1)], Adam F. Forrest[(2)], Maria Ana Cataluna[(2)], Michel Krakowski[(3)], Paolo Bardella[(1)]

[(1)] *Dipartimento di Elettronica e Telecomunicazioni, Politecnico di Torino, I-10129, Turin, Italy*
[(2)] *Institute of Photonics and Quantum Sciences, Heriot Watt University, Edinburgh, EH14 4AS, United Kingdom*
[(3)] *III-V Lab, 1 Avenue Augustin Fresnel, Campus de Polytechnique, 91767 Palaiseau, France*

Abstract: We numerically study a tapered chirped Quantum Dot Semiconductor Optical Amplifier operating in the 1100 nm–1350 nm wavelength range, showing good agreement with experiments in terms of pulse amplification in both the single- and double-pass setups.

1. Introduction

Chirped tapered Quantum Dot (QD) Semiconductor Optical Amplifiers (SOAs) are a key solution for the direct amplification of ultra-short pulsed sources such as mode-locked lasers, thanks to their broad gain bandwidth and fast recovery times. The introduction of the layers of QDs emitting at various wavelength ("chirping") allows an accurate design of the broadening of the device bandwidth, while the tapered configuration allows to reduce saturation effects under large current operation and helps maintaining a high quality output field profile. Traditionally, SOAs are operated in a so-called single-pass configuration, where light is injected at one facet of the amplifier and extracted from the other, with amplification occurring over a single passage through the device. However, a double-pass configuration, where the light is reflected back in the amplifier by an external mirror, can lead to enhanced performances, increasing the output power of the optical signal, with a limited degradation of the amplified pulses duration. This second configuration is therefore a possible future standard for the amplification of light sources [1]. In this study, we simulate a chirped tapered multi-section device using a time-domain travelling-wave (TDTW) model, in order to asses the advantages of the double-pass solution with respect to the single-pass one.

The device under analysis is 6 mm long, with an initial 14 µm wide straight ridge waveguide (rear of the device), followed by a first tapered section with a full taper angle of 3°, and finally a second tapered section with a full taper angle of 0.8°, amounting to a total width of 110 µm at the front facet. At 1.875 mm from the rear facet, an insulation trench was etched, creating two bias sections that can be driven independently for greater flexibility. The active material is composed of 10 chirped InAs QD layers: three layers with Ground State (GS) emission λ_{GS} centered at 1243 nm, three at 1211 nm, and four at 1285 nm [2].

2. Numerical Model

The numerical model employed is an enhancement of the TDTW model proposed in [3], modified to include the chirped nature of the QD active medium, the stimulated emission from the second QD excited state ES2, and the external feedback mirror for double-pass amplification. A set of Multi-Population Rate Equations (MPRE) describes the dynamics of the number of carriers in the Separate Confined Heterostructure and in the Wetting Layer and of the occupation probabilities in the confined QD energy levels (ES2, ES1 and GS), taking into account scattering and recombination phenomena. The field propagation, instead, is described by means of two wave equations associated with the forward and backward components of the field:

$$\frac{1}{v_g}\frac{\partial E^{\pm}}{\partial t} \pm \frac{\partial E^{\pm}}{\partial z} = -\frac{1}{2}(\alpha_i^{\pm}(z)+\alpha_p)E^{\pm}(z,t) - j\frac{\omega_0 \Gamma_{xy}^{\pm}(z)}{2cn_{eff}\varepsilon_0}P^{\pm}(z,t) + S_{sp}^{\pm}(z,t) \tag{1}$$

with v_g group velocity, $E^{\pm}$ progressive and regressive components of the field, α_p plasma losses, ω_0 reference angular frequency, n_{eff} effective index. The intrinsic waveguide losses $\alpha_i^{\pm}(z)$ and the transverse confinement factor $\Gamma_{xy}^{\pm}(z)$ vary with respect to the position and have different behaviors depending on the propagation direction in this tapered structure [2] due to the weak confinement of the field in the transverse direction. $P^{\pm}(z,t)$ is the macroscopic polarisation, linked to the stimulated response of the system, and $S_{sp}^{\pm}(z,t)$ describes its spontaneous emissions.

Boundary conditions are required for (1) in order to take into account the external optical injection and the reflection that occurs when operating in the double-pass configuration [4]:

$$E^{+}(0,t) = r_0 E^{-}(0,t) + \sqrt{1-r_0^2}E_{\text{inj}}(t) \tag{2}$$

$$E^{-}(L,t) = r_L E^{+}(L,t) + (1-r_L^2)r_{\text{ext}}E^{+}(L,t-\tau_{\text{ext}}) \tag{3}$$

with r_0 and r_L residual reflectivities in the facets of the device (both assumed to be 10^{-5}), $E_{\text{inj}}(t)$ external injected field, r_{ext} reflectivity of the external mirror, and τ_{ext} propagation delay of the external cavity.

3. Simulation Results

An example of simulated photo-luminescence spectrum, calculated at the front facet without external optical sources for $I_{\text{Front}} = 5\,\text{A}$ and $I_{\text{Rear}} = 0.1\,\text{A}$, is presented in Fig. 1a; the two peaks visible in the spectrum are due to linear combination of the emission coming from the confined states of the chirped layers. In addition, the considered TDTW method allows us to easily calculate the internal distribution of optical net gain, shown as contour map in Fig. 1b, which clearly highlights the effect of the non-uniform current injection; for the considered combination of currents, the high gain profile remains homogeneous throughout the second tapered section in its entirety, despite the high driving currents. This information offers significant possibilities for an optimization of the device performances.

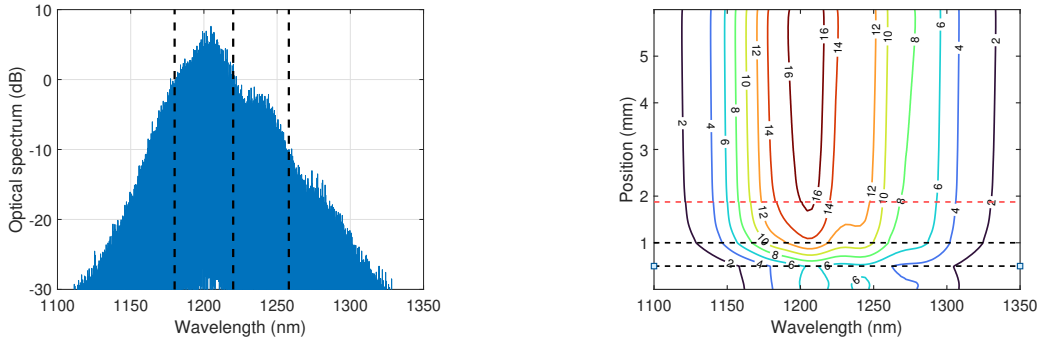

(a) **(b)**

Fig. 1. **(a)** Photo-luminescence spectrum at the front facet, for $I_{\text{Front}} = 5\,\text{A}$ and $I_{\text{Rear}} = 0.7\,\text{A}$; the vertical dashed lines indicate the wavelengths of the injected signals. **(b)** Optical gain (cm^{-1}) spectral map contours for $I_{\text{Front}} = 5\,\text{A}$ and $I_{\text{Rear}} = 0.7\,\text{A}$. The black dashed lines separate the three sections of the SOA, while the red line shows the position of the insulation trench.

In Fig. 2a we report the single-pass and double-pass amplification evaluated sending in input a train of Gaussian pulses centered at 1258 nm with average power of 2.5 mW, Full width at Half Maximum 2.3 ps and repetition rate of 5 GHz. Simulations are repeated for the rear section current ranging from 100 mA to 700 mA, and a front section current in the 1 A-5 A range. The double-pass configuration clearly offers increased amplification relative to the single-pass case without significantly affecting the width of the pulses. The maximum outright enhancement is 4.1 dB for $I_{\text{Front}} = 5\,\text{A}$ and $I_{\text{Rear}} = 0.1\,\text{A}$. These findings are in good agreement with the experimental evidences [2].

Finally, we analyzed the SOA capabilities for different input signal wavelengths (Fig. 2b). In this case, it is clear that the device can provide significant amplification even for $\lambda = 1180\,\text{nm}$ and $\lambda = 1220\,\text{nm}$; however, saturation effects begin to appear when using a double-pass setup, which limits the increase in the available optical gain.

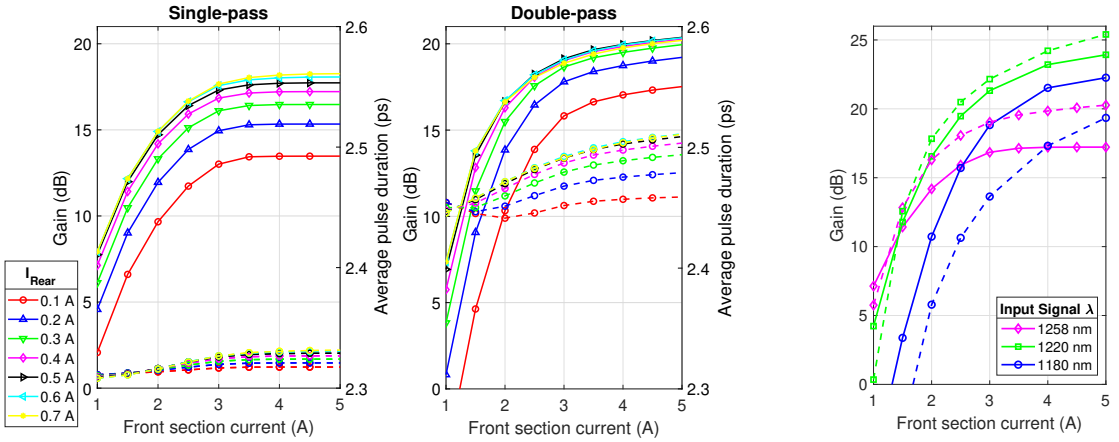

(a) **(b)**

Fig. 2. **(a)** Amplification (left axis) and pulse duration (right axis) in single- and double-pass configuration for an input signal at 1258 nm. **(b)** Amplification in single- (solid) and double- (dashed) pass configuration for different injected source wavelengths; $I_{\text{Rear}} = 0.4\,\text{A}$.

The TDTW results confirm the experimental evidence that the double-pass configuration offers promising enhancement of the gain and its bandwidth with respect to the canonical single-pass case.

References

[1] A. F. Forrest, et al., Opt. Express **27**, 30752–30762 (2019).

[2] A. F. Forrest, et al., Opt. Express **28**, 846–859 (2020).

[3] M. Rossetti, et al., IEEE J. Quantum Electr. **47**, 139–150 (2011).

[4] A. F. Forrest, et al., in *NUSOD,* , vol. 2021- (2021), pp. 17–18.